THE JOURNAL OF PHYSICAL CHEMISTRY Letters

pubs.acs.org/JPCL Letter

Colloidal Assembly of Au–Quantum Dot–Au Sandwiched Nanostructures with Strong Plasmon–Exciton Coupling

Yi Luo, Yongchen Wang, Muqiong Liu, Hua Zhu, Ou Chen, Shengli Zou, and Jing Zhao*

Cite This: J. Phys. Chem. Lett. 2020, 11, 2449–2456 Read Online

ACCESS | Metrics & More | Article Recommendations | Supporting Information

ABSTRACT: Strong plasmon–exciton coupling could occur in hybrid metal–dye/semiconductor nanostructures, where the fast energy exchange between plasmons and excitons leads to two new eigenmodes of the system, known as Rabi splitting. In experiments, strongly coupled nanosystems are difficult to obtain because they require some strict conditions, such as low plasmonic damping, small plasmon mode volume, and good spectral overlap. This work demonstrates strongly coupled metal–semiconductor nanostructures can be constructed using colloidal assembly. Specifically, sandwiched Au–quantum dot–Au nanostructures were created through the assembly of Au nanoparticles and colloidal quantum dots (QDs). The sizes of the QDs and the assembly conditions were varied to control the mode volume of the plasmonic cavity formed between the two Au nanoparticles. With a decreased gap size, Rabi splitting was observed in both dark-field scattering and fluorescence spectra of single Au–QD–Au nanostructures. Theoretical simulations revealed that the strong coupling occurred between the excitons and the octupolar plasmon modes.

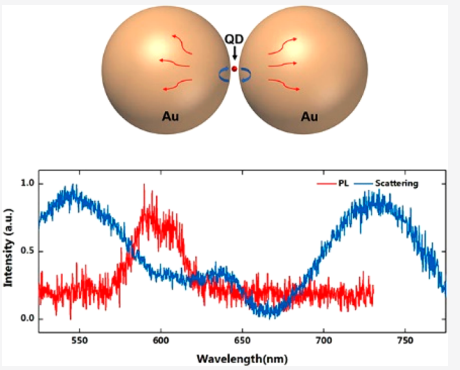

Plasmon–exciton interaction in hybrid metal–quantum emitter nanostructures leads to various unique optical properties. Weak plasmon–exciton interaction arises when plasmonic nanostructures are placed near quantum emitters, which in turn modulates the light absorption and emission properties of the quantum emitters. A number of biosensors, imaging probes, and photovoltaic devices have been developed on the basis of the weak interaction effect.[1−3] While weak coupling occurs relatively easily, strong coupling requires more stringent conditions.[4] To achieve strong coupling, the rate of energy exchange between the plasmon and the exciton needs to be maximized so it can exceed the decay rate of both the plasmon and the exciton. Under this condition, the energy coherently oscillates between the plasmon and exciton, resulting in a plexcitonic state featuring two new eigenmodes. These unique properties make the strongly coupled plasmon–exciton systems promising candidates in many applications such as thresholdless polariton lasing, solar cells, single-photon nonlinear optics, and quantum information processing.[5−15]

The coupling strength (g) between the plasmon and exciton is affected by the plasmon and exciton decay rates, their resonance frequency and oscillator strength, the number of excitons, and the plasmon mode volume (V). So far, strong coupling in complexed systems has been successfully realized by incorporating either multiple excitonic molecules or nanoparticles into plasmonic nanostructures or/and reducing the plasmon mode volume via creating gaps or extra sharp plasmonic features. Strong plasmon–exciton coupling showing splitting in both dark-field scattering and fluorescence spectra was first realized experimentally in a system composed of Ag nanoparticles (NPs) and molecular J-aggregates.[16] In a few exciting recent studies, strong coupling has also been observed by incorporating single colloidal quantum dots (QDs) between a Au NP and a Ag substrate, where a plasmonic gap was formed at the junction between the Au NP and the Ag substrate.[17] Colloidal QDs are particularly attractive for developing a strongly coupled system due to their large absorption cross section and long exciton lifetime compared to those of many molecular dyes. Moreover, the strength of the coupling between QDs and metal NPs could easily be tuned by their size, composition, and spatial geometric arrangement. So far, the few strongly coupled QD–metal systems relied on creating a gap plasmon between a metal NP/tip and a metal substrate.[14,15,17,18] A substrate-free system that could be solution-processed will make them for suitable building blocks for optoelectronic devices and thus is beneficial for future applications.

Assembly of metal NPs and QDs in a colloidal solution offers the possibility of generating a strongly coupled metal NP–QD system with nanometer precision and well-defined structures.[19−21] However, due to the difference in the chemical nature of QDs and metal NPs (MNPs), there is not yet a

Received: January 13, 2020
Accepted: March 10, 2020
Published: March 10, 2020

https://dx.doi.org/10.1021/acs.jpclett.0c00110
J. Phys. Chem. Lett. 2020, 11, 2449–2456

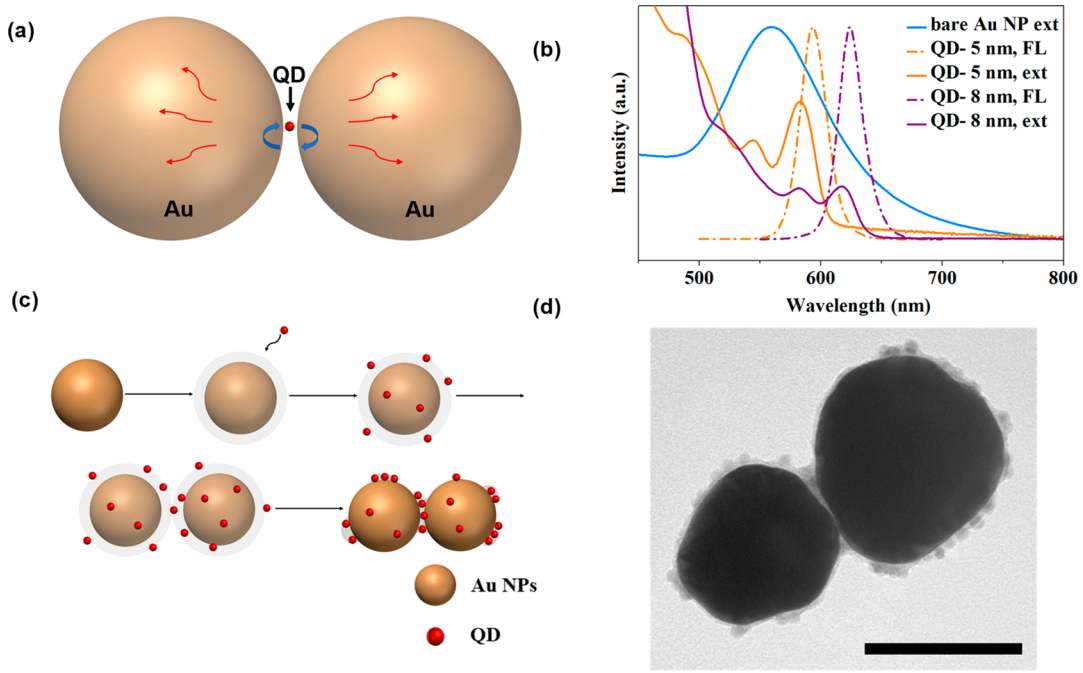

Figure 1. (a) Schematic illustration of strong plasmon−exciton coupling in a Au−QD−Au sandwiched structure. (b) Extinction and fluorescence spectra of Au nanoparticles, 8 nm CdSe/CdS QDs, and 5 nm CdSe/CdS QDs. (c) Schematic illustration of colloidal assembly of Au nanoparticles and QDs. (d) Representative TEM image of the assembled Au−QD−Au nanostructure. The scale bar is 100 nm.

successful method of assembling MNP−QD structures to exhibit a strong coupling effect. Theoretical simulations showed Au or Ag NP dimer structures with CdSe-based QDs sandwiched between the metal NPs have the potential to allow strong coupling between the plasmon and excitons to occur.[22] Silver NPs have demonstrated a stronger coupling effect when conjugated to dye/QDs because their damping is much weaker than that of Au NPs.[23,24] However, colloidally assembled strong coupling Ag/QD structures have not been realized due to the gradual leach of Ag^+ ions from the Ag NPs in solution.[25] The Ag^+ ions can easily etch QDs and lead to chemical quenching of the excitons.[26] Due to this limitation, Au NPs naturally become the proper candidate to build colloidally assembled hybrid metal/QD structures. To overcome the strong plasmon damping of Au NPs, the hybrid structure is designed to have gap plasmon−exciton coupling. A gap plasmon is known to form between two metal NPs in the proximity of each other or a metal NP near a metal surface. A gap plasmon often has a large electromagnetic-field enhancement and small mode volume, which are desirable for achieving strong plasmon−exciton coupling. In a structure in which QDs are placed in the gap of the Au NP dimer, the localized surface plasmon resonance (LSPR) generated in the Au NPs by the incident light could excite the QDs to create excitons in them. The recombination of the exciton then has a chance to transfer the energy back to the plasmon. To maintain the coherent oscillation of energy between the exciton and plasmon, the Rabi frequency, which also determines the coupling strength, needs to greatly exceed any other damping rate in this system. In this work, our strategy for meeting such conditions and for controlling the plasmon−exciton coupling strength is to build sandwiched Au−QD−Au structures and to tune the size of the gap between the Au NPs (scheme in Figure 1a). Moreover, to establish a structure-oriented performance relationship, a correlated optical-transmission/scanning electron microscopy technique was employed to determine the morphology of the nanostructure studied. Under proper conditions, Rabi splitting was observed in both the dark-field scattering and fluorescence spectra of the Au−QD−Au structures, confirming that a strongly coupled system was created via colloidal assembly. Theoretical simulations revealed that the strong coupling in our system occurred between the high-order octupolar plasmon mode of the Au NP dimers and the exciton of the QDs.

Gold NPs and CdSe/CdS core/shell QDs of the desired sizes were synthesized according to previous literature and applied as the building blocks to produce the Au−QD−Au sandwich structures.[27,28] To observe the coupling between the plasmon of the Au NPs and the exciton of QDs, 100 nm Au NPs and 8 nm CdSe/CdS core/shell QDs were first tested, and their extinction and fluorescence spectra are shown in Figure 1b. Because the QDs were dispersed in hexane whereas the Au NPs were dispersed in water, the QDs were modified with poly(ethylene glycol) methyl ether thiol (PEG-SH) and transferred into water prior to the assembly. For the QDs to attach to the Au NPs, the Au NPs were coated with a thin (3-aminopropyl)triethoxysilane (APTES)-doped silica layer using a previously published method to provide binding sites for the QDs (scheme shown in Figure 1c).[29] The QDs were then mixed with the Au@silica core@shell NPs and stirred overnight. The PEG chains on the QD surface interact with the silica layer on the Au NP through hydrogen bonding and allow the QDs to attach to the Au NPs. Meanwhile, the amine groups from APTES on the silica surface of one Au NP could interact with the negatively charged $Si-O^-$ on the surface of another Au NP and induce the Au−silica−QD structures to aggregate and form dimers. The sample was stirred for 24 h, and the silica shell partially dissolved during stirring and became thinner (see Figure S1). Figure 1d shows a representative TEM image of Au dimers with QDs. The

https://dx.doi.org/10.1021/acs.jpclett.0c00110
J. Phys. Chem. Lett. 2020, 11, 2449−2456

large dark spherelike particles are Au NPs, and the small gray spheres on the Au NP surface are QDs. The gray layer around the Au NPs is partially dissolved silica. A sparse layer of QDs could be observed on the Au NPs, proving that the Au−QD−Au structures indeed formed. Some of the QDs were not in the gap between the two Au NPs but on the outside surface instead. The fluorescence from these QDs is likely quenched by the Au NPs, according to a number of previous studies.[30,31] A control experiment was performed with QDs attached to isolated Au NPs, and no fluorescence from this sample was observed (Figure S2). Therefore, we do not expect them to contribute much to the plasmon−exciton coupling.

The optical properties of individual Au−QD−Au structures were examined under a dark-field microscope, and the correlated structural information was collected by a transmission electron microscope (TEM). Briefly, the Au−QD−Au structures were drop-casted on a labeled TEM grid, and the corresponding dark-field scattering image and TEM image were compared and correlated (Figure S3). Figure 2 shows the

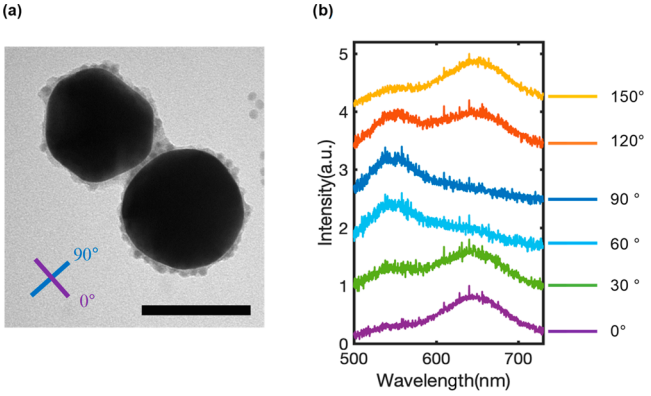

Figure 2. (a) TEM image of a Au−QD−Au structure and (b) its single-particle dark-field scattering spectra under polarized light with varying polarization.

TEM image of a representative Au−QD−Au structure and the corresponding dark-field scattering spectra with varying incident light polarization. The single-particle dark-field scattering spectra showed two distinct peaks whose relative intensity changed when the polarization of the incident light changed. This behavior matches well with the previously observed plasmonic coupling between two metal NPs, suggesting that the peaks originated from the plasmonic coupling effect. Therefore, intermediate or strong plasmon−exciton coupling did not occur in the current structures, likely due to the relatively large gap size (4.2 nm measured from the TEM image in Figure 2a) of these structures. We notice that the gap size measured from the TEM image is smaller than the diameter of the QDs. This discrepancy likely arises for two reasons. (1) The gap size is calculated on the basis of the two nearest points between the Au NPs in the TEM image, which is a two-dimensional projection of the three-dimensional assembled structure. It does not necessarily represent the three-dimensional structure. (2) The position of the QDs may be offset from the center of the gap, which will decrease the shortest distance between the two Au NP surfaces. In addition, Au NP dimers without QDs were synthesized as a control, and their scattering spectra and corresponding scanning electron microscope (SEM) images are included in Figure S4. The spectra showed patterns and peak positions similar to those of the spectra of the Au−QD−Au assemblies, which confirms that the scattering spectra of weakly coupled Au−QD−Au structures are dominated by the scattering of Au NP dimers.

The plasmonic mode volume has a major impact on the plasmon−exciton coupling strength, where the coupling strength (g) increases with a decrease in the mode volume V ($g \propto \sqrt{1/V}$). In our design, the mode volume can be reduced by shortening the distance between the Au NPs and decreasing the diameter of the QDs. In the following experiments, 5 nm CdSe/CdS QDs functionalized with PEG-SH were mixed with Au@silica NPs and assembled onto them via stirring. The silica shell thickness and the amount of QDs were further reduced to shorten the distance between the two Au NPs. After incubation for 12 h, the silica layer completely disappeared in the TEM image of the Au−QD−Au structure and the size of the gap between the Au NPs becomes too small to measure (Figure S5a). However, the QDs are hardly visible in this structure, due to the much smaller size of the QDs, the lower electron diffraction efficiency of CdSe/CdS compared to that of Au, and the low QD:Au ratio. To confirm the QDs were indeed conjugated to the structure, a fluorescence image of individual Au−QD−Au structures dispersed on a thin glass slide was collected and compared with its dark-field scattering image (panels b and c, respectively, of Figure S5). Only the spots that appeared in both images were further examined.

Figure 3 shows the dark-field scattering and photoluminescence (PL) spectra of a representative Au−QD−Au

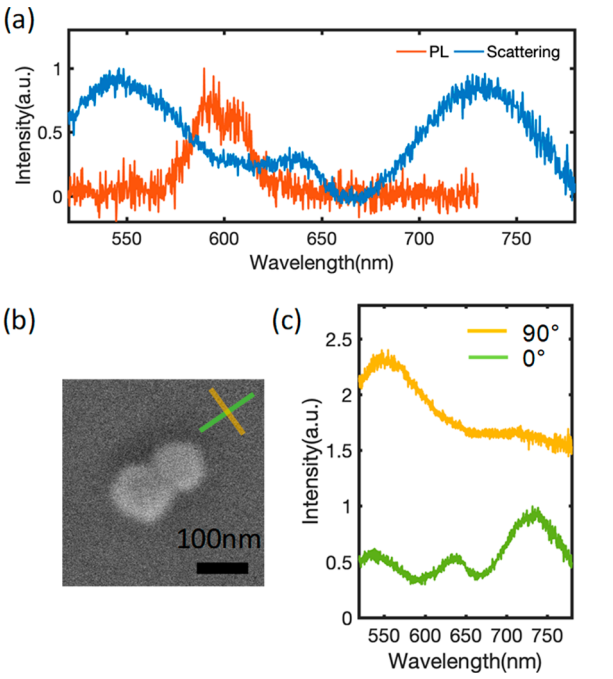

Figure 3. (a) Unpolarized dark-field scattering and PL spectra of a Au−QD−Au structure, (b) its SEM image (scale bar of 100 nm), and (c) polarized scattering spectra of the structure.

structure and its morphology imaged using SEM. Another example is listed in Figure S6. SEM correlation was used instead of TEM correlation because the carbon support film on the TEM grid introduced background fluorescence and made it difficult to observe the signal from the QDs. Three peaks were observed in the dark-field scattering spectra under unpolarized white light excitation. In addition, the PL spectrum collected

https://dx.doi.org/10.1021/acs.jpclett.0c00110
J. Phys. Chem. Lett. 2020, 11, 2449−2456

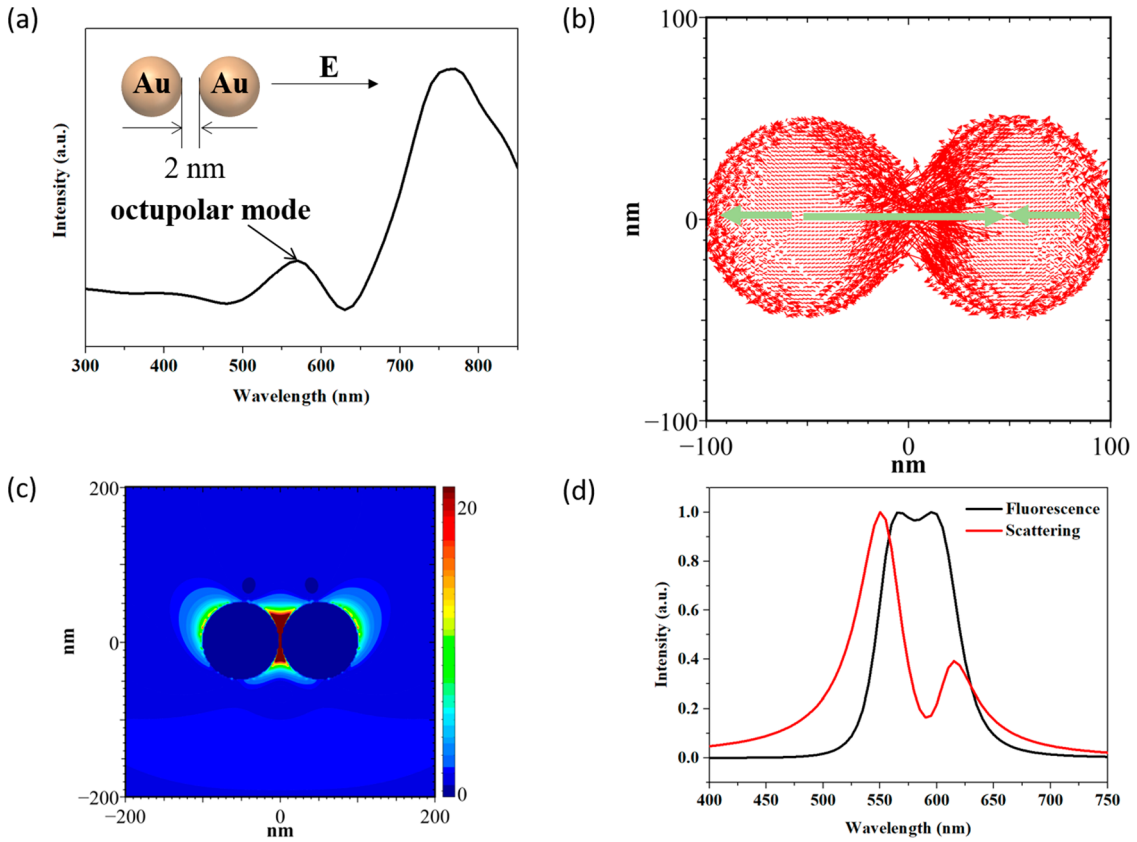

Figure 4. (a) Scattering spectrum of a Au dimer that consisted of two 100 nm Au spheres with a 2 nm gap between them. (b) Dipole distribution of the Au dimer excited at 570 nm. (c) Electric-field distribution of the Au dimer excited at 570 nm. (d) Simulated fluorescence and scattering spectra of the Au−QD−Au structure.

from the same nanostructure excited at 405 nm exhibited a split in the peak, which is a signature of Rabi splitting due to the strong interaction between the plasmon and exciton. The same Rabi effect could also cause a splitting in the dark-field scattering spectrum. However, the origin of the spectral feature in the scattering spectrum of the structure needs to be considered more carefully. For normal Au NP dimers, two peaks are expected in their scattering spectra, which arise from the transverse and longitudinal modes due to the dipole−dipole interaction between the two NPs. The longitudinal mode is usually at a wavelength much longer than that of the LSPR of individual Au NPs, whereas the transverse mode remains at a similar wavelength. Moreover, when the polarization of light is parallel (or perpendicular) to the axis defined by the centers of the two Au NPs, only one longitudinal (or transverse) peak is expected to appear. Thus, polarized light was used to excite the structure to examine how the transverse/longitudinal plasmon mode interacts with the excitons of the QD. When the polarization is perpendicular to the axis, one intense peak at ∼580 nm was observed (yellow spectrum in Figure 3c), which is attributed to the transverse mode. When the polarization aligns with the axis, three peaks were observed instead of one (green spectrum in Figure 3c). The peak at 720 nm is assigned to the longitudinal mode. However, the origin of the other two peaks at 530 and 640 nm is different and likely due to plasmon−exciton coupling, which is further explained below.

Because the exciton of the 5 nm QDs is in resonance with the transverse mode, the possibily of coupling the exciton to the transverse mode is first considered. However, the coupling is ruled out for the following reasons. First, the discrete dipole approximation (DDA) method[32] was applied to simulate the electric-field distribution around a Au dimer that consisted of two 100 nm Au NPs. The simulation reveals that the electric-field enhancement of the transverse mode is weak, which is undesired for plasmon−exciton coupling. Second, the largest enhancement occurred above and below the individual Au NPs instead of in the gap from our calculations (see Figure S7) and previous literature.[33] Thus, the plasmon mode volume is large, which decreases the plasmon−exciton coupling strength. Moreover, the transverse mode is independent of the gap between the Au NPs. If this mode could couple strongly to the excitons, strong coupling should have been observed in the structure shown in Figure 2b, which contradicts the experimental results. Therefore, we searched for other plasmon modes, which depends on the gap size. Notice the Au NPs in our system are fairly large (∼100 nm in diameter); they could exhibit a higher-order plasmon mode that matches the exciton energy and couples to it.[34] To examine this hypothesis, electrodynamics simulations using the DDA method were carried out. Figure 4a shows the simulated scattering spectrum of a Au NP dimer that consisted of two 100 nm Au nanospheres with a gap of 2 nm. Two peaks at 570 and 765 nm appeared in the scattering spectrum when the dimer was excited by light that was polarized along the longitudinal direction of the dimer. The electric-field vector plots of the two peaks (in Figure 4b and Figure S8) showed that the mode at 570 nm arises from an octupolar mode, while the peak at 765 nm is the longitudinal dipole mode. The 570 nm peak dissappears when the gap size is >4 nm, acoording to the DDA

https://dx.doi.org/10.1021/acs.jpclett.0c00110
J. Phys. Chem. Lett. 2020, 11, 2449−2456

simulations (Figure S9). Figure 4c shows the electric-field distribution of the octupolar mode. The highest electric field is observed at the gap between the Au nanospheres. Because the resonance wavelength of the octupolar mode matches well with the fluorescence peak wavelength of the QDs (~594 nm), it is likely to couple to the excitons. The coupling between the octupolar plasmon mode and the exciton is further simulated with a semianalytical solution using equations in ref 17 (see details in Experimental Methods). Figure 4d shows that when coupling strength g was adjusted to 185 meV, peak splitting was observed in both the scattering and the fluoresence spectra. The position and line shape of the splitted peaks match qualitatively with the experimentally observed spectra in Figure 3a, proving that strong coupling did occur between the exciton and the octupolar plasmon in the Au−QD−Au system. The results revealed that the critical factor that determines the plasmon−exciton coupling strength in the Au−QD−Au structures is the mode volume, or the gap size.

In conclusion, strongly coupled metal−semiconductor hybrid nanostructures were synthesized by the colloidal assembly of Au NPs and CdSe/CdS QDs with proper surface functionalization. To achieve strong plasmon−exciton coupling, a Au NP dimer structure in which QDs were sandwiched between two Au NPs was employed. A gap plasmon emerged between the Au NPs, and its mode volume was affected by the gap size. In the structures with a larger gap size, no peak splitting was observed because the energy exchange between the plasmon and exciton was not fast enough to overcome the plasmon damping and exciton decay. With a much smaller gap size of ~2 nm, both the dark-field scattering and the fluorescence of the Au−QD−Au structure showed a Rabi splitting effect, because of the strong coupling between the octupolar plasmon mode and the excitons. This work demonstrates the ability of colloidal assembly methods to control the nanoscale spatial arrangement of colloidal NPs and therefore to modulate the plasmon−exciton coupling strength. In the future, the methods will be further optimized to improve the yield of the assembled structures and apply them in optoelectronic devices. Efforts will also be devoted to study the plasmon−exciton interaction mechanism in assembled QD−Au NP oligomers.

EXPERIMENTAL METHODS

Chemicals. Gold(III) chloride trihydrate (≥99.9% trace metal basis), hydroxylamine hydrochloride, 2-propanol (ACS reagent, ≥99%), 3-mercaptopropionic acid (MPA) (≥99%), tetraethyl orthosilicate (TEOS) (≥99.0%), 1-octadecene (ODE, 90%), 1-octanethiol (OCT, >98.5%), trioctylphosphine oxide (TOPO, 99%), trioctylphosphine (TOP, 97%), oleic acid (OLA, 90%), and oleylamine (OAm, 70%) were purchased from Sigma-Aldrich. Poly(ethylene glycol) methyl ether thiol (PEG-SH) (average M_n = 5000 g/mol) was purchased from Polymer Source. Sodium citrate dehydrate was purchased from Fisher Scientific. Cadmium oxide (CdO, 99.998%), selenium powder (Se, 99.999%), and octadecylphosphonic acid (ODPA) were purchased from PCI. Ammonium hydroxide (28.0−30.0%) was purchased from J. T. Baker. All chemicals were used as received.

Au Nanoparticle Synthesis. The 100 nm Au nanoparticle was synthesized following a published procedure with slight modification.[28] First, 40 nm Au nanoparticles were synthesized as the seeds following Frens' method.[35] Then, 53 mL of distilled water was added to a round-bottom flask under vigorous stirring followed by the addition of 6 mL of the previously prepared 40 nm Au seeds. After 2 min, 900 μL of a sodium citrate solution (0.0388 M) was added to the flask dropwise. After an additional 2 min, 0.8 mL of $HAuCl_4$ (0.0254 M) was added to the flask. Finally, after an additional 2 min, 1.3 mL of a hydroxylamine hydrochloride solution (0.0101 M) was added dropwise and the round-bottom flask was removed from the stir plate after 2 h.

QD Synthesis and Phase Transfer. The method reported by Chen et al. was adopted to synthesize the CdSe/CdS QDs with minor modifications.[27] For synthesis of the CdSe core, briefly, 60 mg of CdO, 280 mg of ODPA, and 3.0 g of TOPO were added to a 50 mL flask. The mixture was heated to 150 °C and degassed under vacuum for 1 h. Under a nitrogen flow, the reaction mixture was further heated to 320 °C to form a colorless solution. After 2.0 mL of TOP had been added to the solution, the temperature was quickly increased to 380 °C, at which point a Se/TOP (60 mg of Se in 0.5 mL of TOP) solution was injected quickly into the flask. When the CdSe core QDs reached the desired size, the reaction was terminated by removing the heat. After the mixture had cooled to room temperature, the resulting CdSe QDs were precipitated by adding acetone and redispersed in hexane for further uses.

For CdS shell growth, a hexane solution containing 400 nmol of CdSe core QDs was loaded in a mixture of 4.0 mL of ODE and 4.0 mL of OAm. The reaction solution was degassed under vacuum at room temperature for 1 h and 120 °C for an additional 20 min to completely remove the hexane, water, and oxygen inside the reaction solution. Then, the reaction solution was heated to 240 °C, at which point a desired amount of cadmium(II) oleate [2 monolayers (MLs) for 5 nm QD and 4 MLs for 8 nm QD, diluted in 4.0 mL of ODE] and 1.2 equiv of OCT (diluted in 4.0 mL of ODE) were injected into the growth solution at a rate of 2 ML/h using a syringe pump. Meanwhile, the reaction temperature was further increased to 310 °C and maintained for the rest of the reaction. During the growth, 1.0 mL of OLA was injected every hour. After the precursor infusion had reached completion, an additional 1.0 mL of OLA was quickly injected and the solution was further annealed at 310 °C for 10 min. The resulting CdSe−CdS core−shell QDs were precipitated by adding acetone and then redispersed in chloroform as a stock solution.

After synthesis, the QDs were functionalized with PEG-SH and transferred into water. Briefly, 10 mg of PEG-SH was dissolved in 5 mL of chloroform. Then, 2 mL of QDs dispersed in chloroform (3 mg/mL) was added to the PEG-SH solution dropwise. The solution was stirred overnight. After 12 h, hexane was added to the solution to precipitate the QDs and the mixture was centrifuged at 5000 rpm for 15 min. The supernatant was discarded, and methanol was added to dissolve the QDs. Finally, the methanol was dried under N_2 gas blowing, and the dried QDs were dispersed in 8 mL of water.

Au@Silica Synthesis. Au@silica core@shell structures were synthesized according to the method developed by Chen et al.[36] Six milliliters of the 100 nm Au nanoparticles in water was concentrated to 3 mL of a solution by centrifugation and then transferred into 15 mL of 2-proponal; 120 μL of 3-mercaptopropionic acid (5 mM in ethanol) were then added to the solution. The mixture was allowed to stir for 30 min. Four microliters of tetraethyl orthosilicate, 3 μL of (3-aminopropyl)triethoxysilane, and 540 μL of ammonium hydroxide were then added. The reaction mixture was kept

https://dx.doi.org/10.1021/acs.jpclett.0c00110
J. Phys. Chem. Lett. 2020, 11, 2449−2456

at room temperature for 1 h, centrifuged thrice, and finally dispersed in 3 mL of DI water.

Au−QD−Au Assembly. Fifty microliters of the QD−PEG-SH solution was added to 3 mL of the Au@silica solution. The mixture was allowed to stir for 12 h to ensure sufficient dissolution of silica. As a result, Au−QD−Au structures formed.

Preparation of Samples for Electron Microscopy. For TEM correlation, the Au−QD−Au solution was diluted 10-fold with DI water and 4 μL of the diluted sample was drop-casted on a TEM grid. The grid was left in open air to dry. This sample was then used for single-particle optical measurement as well as TEM imaging.

For SEM correlation, the Au−QD−Au solution was diluted 10-fold with ethanol and 4 μL of the diluted sample was drop-casted on a glass slide. The glass slide was left in open air to dry. A copper reference grid was glued to the glass slide to help locate the particles under SEM imaging. This sample was then used for single-particle optical measurement as well as SEM imaging.

Single-Particle Optical Study and TEM/SEM Correlation. The sample was examined under a Nikon Ti-u microscope with an unpolarized/polarized halogen lamp. The dark-field condenser (NA 0.85) was adjusted to focus the incident light at the specimen plane. The scattered light was focused by a 100× NA 0.8 oil immersion objective (variable NA 0.8−1.3) and then passed through a manually controlled slit to the spectrograph (Isoplane SCT 320, Princeton Instruments) equipped with a CCD camera (PIXIS 1024 BR, Princeton Instruments). Single-particle scattering spectra were collected by narrowing the slit and selecting the proper area of interest. The spectrum correction was carried out by subtracting the background and then dividing the lamp signal collected from the nearby area with no particles. The TEM grid was then examined with an FEI Tecnai G2 Spirit BioTWIN instrument to locate the particles and acquire the TEM images.

To measure the single-structure fluorescence, the prepared glass slide was placed under the microscope with a 405 nm pulsed laser (Picoquant) sent through the objective to excite the sample. The emitted photon was focused by the same objective and sent to the spectrometer as described above. The glass slide was thereafter examined with an FEI Nova NanoSEM 450 instrument to acquire the SEM images.

Simulations. The scattering spectrum and electric-field contour plot of Au nanoparticles were calculated using the DDA method.[32] The dielectric constants of Au were taken from ref 37.

To simulate the spectral features due to plasmon−exciton interaction, we applied a semianalytical model.[17] Specifically, the scattering and PL spectra of the Au−QD−Au structure are calculated on the basis of eqs 1 and 2.

$$S(\omega) \propto \omega^4 \left| \frac{{\omega_{QD}}^2 - \omega^2 - i\gamma_{QD}\omega}{(\omega^2 - {\omega_{SP}}^2 + i\gamma_{SP}\omega)(\omega^2 - {\omega_{QD}}^2 + i\gamma_{QD}\omega) - \omega^2 g^2} \right|^2 \tag{1}$$

$$\mathrm{PL}(\omega) = \frac{\gamma_{SP}}{\pi} \left| \frac{-i\left(\frac{g}{2}\right)}{\left[\frac{\gamma_{SP}+\gamma_{QD}}{4} + \frac{i(\omega_{QD}-\omega_{SP})}{2} - i(\omega - \omega_{SP})\right]^2 + \left[\left(\frac{g}{2}\right)^2 + \left(\frac{\omega_{QD}}{2} - \frac{\omega_{SP}}{2}\right)^2 - \left(\frac{\gamma_{SP}}{4} - \frac{\gamma_{QD}}{4}\right)^2\right]} \right|^2 \tag{2}$$

In the equations, ω_{SP} is the plasmon resonance frequecy of 2.19 eV, which is the resonance frequency of the octupole mode as determined by the DDA simulations in Figure 4. The resonance frequency of the QD ω_{QD} is 2.09 eV according to experimental PL spectrum of the QDs in Figure 1b. The damping constants γ of Au and QDs ($\gamma_{SP} = 5.8 \times 10^{13}$, and $\gamma_{QD} = 2.3 \times 10^{13}$ Hz) were extracted from the line width of the spectra in Figure 1b, using the method described in the literature.[38] The details of how the fitting paramaters are obtained are available in the Supporting Information. g is the couping strength that was set to 185 meV (4.5×10^{13} Hz) to match the experimental results. The simulated results in Figure 4 show that both the fluorescence and the plasmon octupolar mode split into two peaks, consistent with what has been observed experimentally.

■ ASSOCIATED CONTENT

Supporting Information

The Supporting Information is available free of charge at https://pubs.acs.org/doi/10.1021/acs.jpclett.0c00110.

Additional TEM images, optical microscopy images and spectra, simulation results, and details of the fitting (PDF)

■ AUTHOR INFORMATION

Corresponding Author

Jing Zhao − *Department of Chemistry, University of Connecticut, Storrs, Connecticut 06269-3060, United States;* orcid.org/0000-0002-6882-2196; Phone: 860-486-2443; Email: jing.zhao@uconn.edu; Fax: 860-486-2981

Authors

Yi Luo − *Department of Chemistry, University of Connecticut, Storrs, Connecticut 06269-3060, United States*

Yongchen Wang − *Department of Chemistry, University of Connecticut, Storrs, Connecticut 06269-3060, United States;* orcid.org/0000-0003-0792-2908

Muqiong Liu − *Department of Chemistry, University of Central Florida, Orlando, Florida 32816-2366, United States*

Hua Zhu − *Department of Chemistry, Brown University, Providence, Rhode Island 02912, United States;* orcid.org/0000-0003-2733-7837

Ou Chen − *Department of Chemistry, Brown University, Providence, Rhode Island 02912, United States;* orcid.org/0000-0003-0551-090X

Shengli Zou − *Department of Chemistry, University of Central Florida, Orlando, Florida 32816-2366, United States;* orcid.org/0000-0003-1302-133X

Complete contact information is available at: https://pubs.acs.org/10.1021/acs.jpclett.0c00110

https://dx.doi.org/10.1021/acs.jpclett.0c00110
J. Phys. Chem. Lett. 2020, 11, 2449−2456

Notes

The authors declare no competing financial interest.

■ ACKNOWLEDGMENTS

J.Z. acknowledges the financial support from a National Science Foundation CAREER AWARD (CHE-1554800) and Grant CBET-1936228. S.Z. acknowledges the Extreme Science and Engineering Discovery Environment (XSEDE) Open Science Grid (OSG) as the service provider through allocation szou. O.C. is thankful for the support from the National Science Foundation (CMMI-1934314 and CBET-1936223).

■ REFERENCES

(1) Li, M.; Cushing, S. K.; Wu, N. Plasmon-Enhanced Optical Sensors: A Review. *Analyst* **2015**, *140*, 386−406.
(2) Enrichi, F.; Quandt, A.; Righini, G. C. Plasmonic Enhanced Solar Cells: Summary of Possible Strategies and Recent Results. *Renewable Sustainable Energy Rev.* **2018**, *82*, 2433−2439.
(3) Yu, H.; Peng, Y.; Yang, Y.; Li, Z.-Y. Plasmon-Enhanced Light−Matter Interactions and Applications. *npj Comput. Mater.* **2019**, *5*, 45.
(4) Luo, Y.; Zhao, J. Plasmon-Exciton Interaction in Colloidally Fabricated Metal Nanoparticle-Quantum Emitter Nanostructures. *Nano Res.* **2019**, *12*, 2164−2171.
(5) Rodriguez, S. R. K.; Feist, J.; Verschuuren, M. A.; Garcia Vidal, F. J.; Gómez Rivas, J. Thermalization and Cooling of Plasmon-Exciton Polaritons: Towards Quantum Condensation. *Phys. Rev. Lett.* **2013**, *111*, 166802.
(6) Nan, F.; Ding, S.-J.; Ma, L.; Cheng, Z.-Q.; Zhong, Y.-T.; Zhang, Y.-F.; Qiu, Y.-H.; Li, X.; Zhou, L.; Wang, Q.-Q. Plasmon Resonance Energy Transfer and Plexcitonic Solar Cell. *Nanoscale* **2016**, *8*, 15071−15078.
(7) Harris, S. E.; Field, J.; Imamoğlu, A. Nonlinear Optical Processes Using Electromagnetically Induced Transparency. *Phys. Rev. Lett.* **1990**, *64*, 1107.
(8) Khitrova, G.; Gibbs, H.; Kira, M.; Koch, S. W.; Scherer, A. Vacuum Rabi Splitting in Semiconductors. *Nat. Phys.* **2006**, *2*, 81.
(9) Christopoulos, S.; von Hogersthal, G. B. H.; Grundy, A. J. D.; Lagoudakis, P. G.; Kavokin, A. V.; Baumberg, J. J.; Christmann, G.; Butte, R.; Feltin, E.; Carlin, J.-F.; Grandjean, N. Room-Temperature Polariton Lasing in Semiconductor Microcavities. *Phys. Rev. Lett.* **2007**, *98*, 126405.
(10) Kolaric, B.; Maes, B.; Clays, K.; Durt, T.; Caudano, Y. Strong Light−Matter Coupling as a New Tool for Molecular and Material Engineering: Quantum Approach. *Adv. Quan. Technol.* **2018**, *1*, 1800001.
(11) Snijders, H.; Frey, J.; Norman, J.; Bakker, M.; Langman, E.; Gossard, A.; Bowers, J.; Van Exter, M.; Bouwmeester, D.; Löffler, W. Purification of a Single-Photon Nonlinearity. *Nat. Commun.* **2016**, *7*, 12578.
(12) Pelton, M.; Storm, S. D.; Leng, H. Strong Coupling of Emitters to Single Plasmonic Nanoparticles: Exciton-Induced Transparency and Rabi Splitting. *Nanoscale* **2019**, *11*, 14540−14552.
(13) Bitton, O.; Gupta Satyendra, N.; Haran, G. Quantum Dot Plasmonics: From Weak to Strong Coupling. *Nanophotonics* **2019**, *8*, 559.
(14) Groß, H.; Hamm, J. M.; Tufarelli, T.; Hess, O.; Hecht, B. Near-Field Strong Coupling of Single Quantum Dots. *Sci. Adv.* **2018**, *4*, No. eaar4906.
(15) Santhosh, K.; Bitton, O.; Chuntonov, L.; Haran, G. Vacuum Rabi Splitting in a Plasmonic Cavity at the Single Quantum Emitter Limit. *Nat. Commun.* **2016**, *7*, 11823.
(16) Wersäll, M.; Cuadra, J.; Antosiewicz, T. J.; Balci, S.; Shegai, T. Observation of Mode Splitting in Photoluminescence of Individual Plasmonic Nanoparticles Strongly Coupled to Molecular Excitons. *Nano Lett.* **2017**, *17*, 551−558.
(17) Leng, H.; Szychowski, B.; Daniel, M.-C.; Pelton, M. Strong Coupling and Induced Transparency at Room Temperature with Single Quantum Dots and Gap Plasmons. *Nat. Commun.* **2018**, *9*, 4012.
(18) Park, K.-D.; May, M. A.; Leng, H.; Wang, J.; Kropp, J. A.; Gougousi, T.; Pelton, M.; Raschke, M. B. Tip-Enhanced Strong Coupling Spectroscopy, Imaging, and Control of a Single Quantum Emitter. *Sci. Adv.* **2019**, *5*, No. eaav5931.
(19) Sheikholeslami, S.; Jun, Y.-w.; Jain, P. K.; Alivisatos, A. P. Coupling of Optical Resonances in a Compositionally Asymmetric Plasmonic Nanoparticle Dimer. *Nano Lett.* **2010**, *10*, 2655−2660.
(20) Wang, Y.; Chen, G.; Yang, M.; Silber, G.; Xing, S.; Tan, L. H.; Wang, F.; Feng, Y.; Liu, X.; Li, S.; Chen, H. A Systems Approach Towards the Stoichiometry-Controlled Hetero-Assembly of Nanoparticles. *Nat. Commun.* **2010**, *1*, 87.
(21) Szychowski, B.; Pelton, M.; Daniel, M.-C. Preparation and Properties of Plasmonic-Excitonic Nanoparticle Assemblies. *Nanophotonics* **2019**, *8*, 517.
(22) Manjavacas, A.; García de Abajo, F. J.; Nordlander, P. Quantum Plexcitonics: Strongly Interacting Plasmons and Excitons. *Nano Lett.* **2011**, *11*, 2318−2323.
(23) Yang, Z.-J.; Antosiewicz, T. J.; Shegai, T. Role of Material Loss and Mode Volume of Plasmonic Nanocavities for Strong Plasmon-Exciton Interactions. *Opt. Express* **2016**, *24*, 20373−20381.
(24) Baranov, D. G.; Wersäll, M.; Cuadra, J.; Antosiewicz, T. J.; Shegai, T. Novel Nanostructures and Materials for Strong Light−Matter Interactions. *ACS Photonics* **2018**, *5*, 24−42.
(25) Sotiriou, G. A.; Meyer, A.; Knijnenburg, J. T.; Panke, S.; Pratsinis, S. E. Quantifying the Origin of Released Ag+ Ions from Nanosilver. *Langmuir* **2012**, *28*, 15929−15936.
(26) Dong, C.; Qian, H.; Fang, N.; Ren, J. Study of Fluorescence Quenching and Dialysis Process of Cdte Quantum Dots, Using Ensemble Techniques and Fluorescence Correlation Spectroscopy. *J. Phys. Chem. B* **2006**, *110*, 11069−11075.
(27) Chen, O.; Zhao, J.; Chauhan, V. P.; Cui, J.; Wong, C.; Harris, D. K.; Wei, H.; Han, H.-S.; Fukumura, D.; Jain, R. K.; Bawendi, M. G. Compact High-Quality Cdse−Cds Core−Shell Nanocrystals with Narrow Emission Linewidths and Suppressed Blinking. *Nat. Mater.* **2013**, *12*, 445.
(28) Tian, X. D.; Liu, B. J.; Li, J. F.; Yang, Z. L.; Ren, B.; Tian, Z. Q. Shiners and Plasmonic Properties of Au Core Sio2 Shell Nanoparticles with Optimal Core Size and Shell Thickness. *J. Raman Spectrosc.* **2013**, *44*, 994−998.
(29) Chen, T.; Chen, G.; Xing, S.; Wu, T.; Chen, H. Scalable Routes to Janus Au- Sio2 and Ternary Ag- Au- Sio2 Nanoparticles. *Chem. Mater.* **2010**, *22*, 3826−3828.
(30) Dey, S.; Zhao, J. Plasmonic Effect on Exciton and Multiexciton Emission of Single Quantum Dots. *J. Phys. Chem. Lett.* **2016**, *7*, 2921−2929.
(31) Samanta, A.; Zhou, Y.; Zou, S.; Yan, H.; Liu, Y. Fluorescence Quenching of Quantum Dots by Gold Nanoparticles: A Potential Long Range Spectroscopic Ruler. *Nano Lett.* **2014**, *14*, 5052−5057.
(32) Draine, B. T.; Flatau, P. J. Discrete-Dipole Approximation for Scattering Calculations. *J. Opt. Soc. Am. A* **1994**, *11*, 1491−1499.
(33) Wen, F.; Ye, J.; Liu, N.; Van Dorpe, P.; Nordlander, P.; Halas, N. J. Plasmon Transmutation: Inducing New Modes in Nanoclusters by Adding Dielectric Nanoparticles. *Nano Lett.* **2012**, *12*, 5020−5026.
(34) Chen, J.-D.; Xiang, J.; Jiang, S.; Dai, Q.-F.; Tie, S.-L.; Lan, S. Radiation of the High-Order Plasmonic Modes of Large Gold Nanospheres Excited by Surface Plasmon Polaritons. *Nanoscale* **2018**, *10*, 9153−9163.
(35) Frens, G. Controlled Nucleation for the Regulation of the Particle Size in Monodisperse Gold Suspensions. *Nature, Phys. Sci.* **1973**, *241*, 20−22.
(36) Chen, T.; Chen, G.; Xing, S.; Wu, T.; Chen, H. Scalable Routes to Janus Au- Sio2 and Ternary Ag- Au- Sio2 Nanoparticles. *Chem. Mater.* **2010**, *22*, 3826−3828.
(37) Palik, E. D. *Handbook of Optical Constants of Solids*; Academic Press: New York, 1985.

https://dx.doi.org/10.1021/acs.jpclett.0c00110
J. Phys. Chem. Lett. 2020, 11, 2449−2456

(38) Wu, X.; Gray, S. L.; Pelton, M. Quantum-dot-induced transparency in a nanoscale plasmonic resonator. *Opt. Express* **2010**, *18*, 23633−23645.

https://dx.doi.org/10.1021/acs.jpclett.0c00110
J. Phys. Chem. Lett. 2020, 11, 2449−2456